Macromolecules

pubs.acs.org/Macromolecules Article

Stability of Frank–Kasper Phases in AB_n Miktoarm Star Polymers with Dispersity in n: Simulations and Experiments

Kodai Watanabe,[#] Duyu Chen,[*,#] Yongsi Zhu, Devon Callan, Glenn H. Fredrickson,[*] and Christopher M. Bates[*]

Cite This: https://doi.org/10.1021/acs.macromol.4c02202 Read Online

ACCESS | Metrics & More | Article Recommendations | Supporting Information

ABSTRACT: Miktoarm star polymers with two or more blocks connected at a common junction are known to stabilize Frank–Kasper phases such as σ and A15 over wide regions of phase space due to arm-number asymmetry. To date, studies on AB_n miktoarm stars in this context have focused on well-defined materials with a precise number of A and B arms. Here, using a combination of self-consistent field theory simulations and experiments, we demonstrate that mixtures of AB_n miktoarm stars with dispersity in the number of B arms per molecule (n) similarly stabilize σ and A15. This insight highlights the utility of a synthetic technique known as μSTAR (miktoarm synthesis by termination after ring-opening metathesis polymerization) that simplifies the synthesis of miktoarm star polymers but inherently produces a mixture of AB_n molecules having a distribution in n.

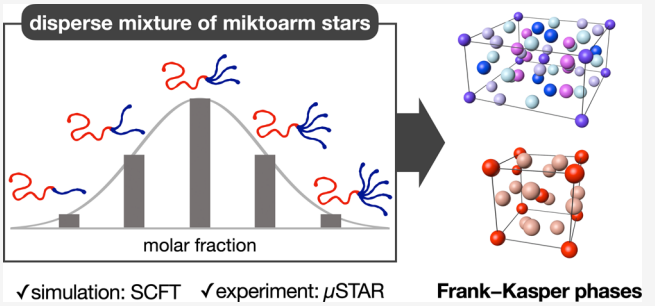

INTRODUCTION

The recent discovery of Frank–Kasper phases[1,2] such as σ[3] and A15[4] in block copolymers has sparked renewed interest in topologically close-packed arrangements of spheres in soft materials.[5−14] For block copolymers, the key design criterion that stabilizes Frank–Kasper phases is known as conformational asymmetry. This concept, which captures the way chains fill space on either side of a block–block interface, can be adjusted through the ratio of block statistical segment lengths (b_A/b_B in a system consisting of A and B monomers)[4,7,15−18] or via architecture.[5−8,17,19,20] For example, the AB_n miktoarm star architecture amplifies differences in statistical segment lengths with arm-number asymmetry (n).[5−7,19] These effects are usually considered together by quantifying the overall degree of conformational asymmetry as a single parameter $\epsilon = n \cdot (b_A/b_B)$,[14,19] which originates from strong-stretching theory.[21] At a given ϵ, the equilibrium phase behavior of AB_n miktoarm stars is also affected by the segregation strength χN_{tot} and volume fraction f_A of A, where χ is the Flory–Huggins interaction parameter, $N_{tot} = N_A + nN_B$ is the total degree of polymerization, and N_A and N_B are the degrees of polymerization of one A and B arm, respectively. Although miktoarm stars represent an intriguing opportunity to readily form and study Frank–Kasper phases, their synthesis remains a significant challenge,[19,22,23] limiting broad access to these unique materials.

Recently, we described a new technique for synthesizing miktoarm star polymers using a combination of ring-opening metathesis polymerization (ROMP) and efficient ene–yne coupling reactions.[24,25] This approach, called μSTAR (miktoarm synthesis by termination after ROMP), is operationally simple, has a wide monomer scope, and is particularly versatile in synthesizing libraries of AB_n-type materials having different numbers of arms (n). A notable difference, however, compared to other synthetic strategies is the inherent dispersity in n that arises from μSTAR—good control over n is always accompanied by a distribution around the average value.

Given the utility of AB_n miktoarm stars in stabilizing Frank–Kasper phases, it is natural to ask whether the same is true of disperse mixtures formed by μSTAR (Figure 1). Here, we demonstrate through a combination of self-consistent field theory (SCFT) simulations and experiments that σ and A15 indeed readily form in disperse mixtures of AB_n miktoarm star polymers. By further amplifying conformational asymmetry through the choice of A = poly(*rac*-lactide) ("L") and B = poly(dodecyl acrylate) ("D") (b_A/b_B = 1.85), well-defined σ and A15 mesophases were obtained in LD_3 and LD_4 systems over a wide range of volume fractions f_L = 0.25–0.39, even in the presence of D arm-number dispersity. Experimentally, order–order phase boundaries deflect to larger f_L as the number of D arms increases; SCFT simulations indicate this

Received: September 12, 2024
Revised: November 16, 2024
Accepted: November 20, 2024

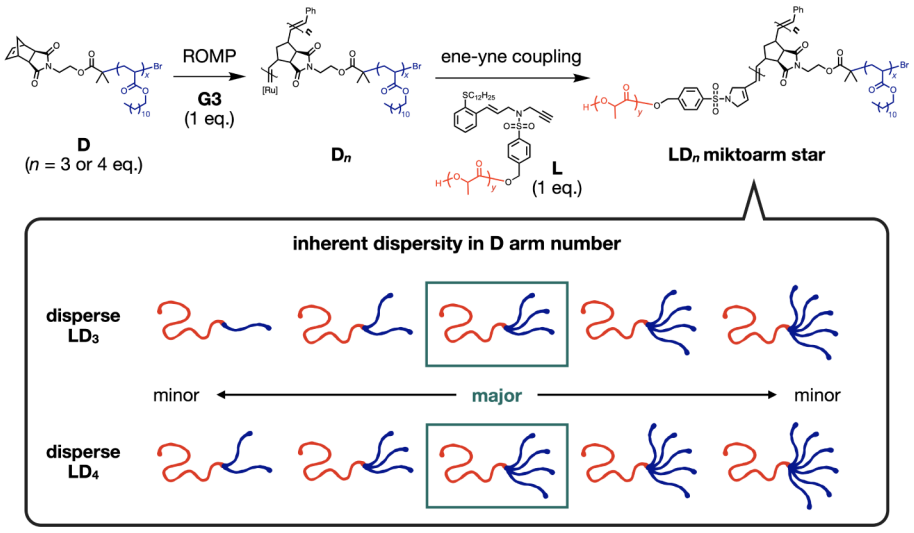

Figure 1. μSTAR readily generates LD$_n$ miktoarm star polymers with inherent dispersity in the number of D arms. Disperse LD$_3$ and LD$_4$ miktoarm stars were investigated to determine whether these systems could stabilize well-defined Frank–Kasper phases.

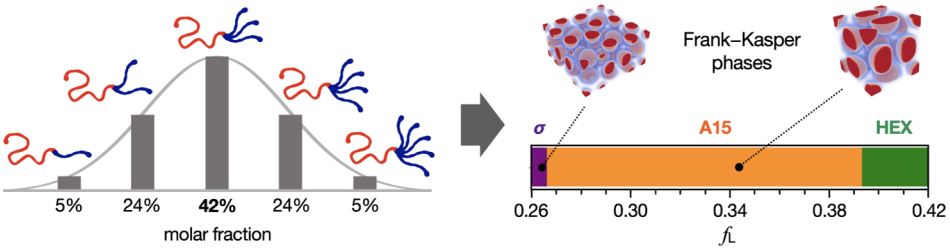

Figure 2. SCFT predicts the σ and A15 phases are stable in melts containing a disperse mixture of LD$_3$ miktoarm stars where the number of B arms per molecule follows a normal distribution. The σ–A15 phase boundary was determined to be $f_L = 0.266$ at $\chi N = 29.30$ and the A15–HEX phase boundary to be $f_L = 0.394$ at $\chi N = 40.00$; N is the degree of polymerization of a single L plus D arm (see Supporting Information for details).

observation provides insight into the opposing effects of each contribution to conformational asymmetry, a shortcoming of strong-stretching theory due to its simplified assumptions. Finally, in situations where ordering is kinetically trapped—a common challenge with architecturally complex block copolymers—we demonstrate that blending a nonselective good solvent significantly improves self-assembly over short time scales. In summary, these results highlight the simplicity and power of μSTAR in creating materials that behave like precise miktoarm star analogues.

RESULTS AND DISCUSSION

Stabilization of σ and A15 Phases in Disperse LD$_3$ Miktoarm Stars. SCFT simulations were first performed to predict how arm-number dispersity impacts the equilibrium phase behavior of AB$_n$ miktoarm star polymers. To mimic LD$_n$ polymers having arm-number asymmetry as well as different statistical segment lengths, a ratio $b_L/b_D = 3.0$ was used in the simulations. This ratio was intentionally selected to be moderately higher than the value measured in experiments (1.85) because SCFT is known to quantitatively overestimate the conformational asymmetry needed to stabilize Frank–Kasper phases.[4,20] A typical molar-mass dispersity of $Đ = 1.10$ was used for the disperse D$_n$ molecules to model well-controlled μSTAR syntheses. To capture the resulting mixture of species, we simulated a melt containing LD, LD$_2$, LD$_3$, LD$_4$, and LD$_5$ at molar fractions of 0.05, 0.24, 0.42, 0.24, and 0.05, respectively, following a normal distribution for the number of D arms (see the Supporting Information for details).

Notably, SCFT simulations indicate the σ and A15 phases are indeed stable in disperse mixtures of LD$_3$ miktoarm stars. Both structures and the window of phase stability are shown in Figure 2. This result suggests appropriately designed miktoarm star polymers synthesized via μSTAR should indeed form Frank–Kasper phases over a relatively wide range of volume fractions, $f_L \approx 0.26$ to 0.39. We also find that the phase behavior of precise and disperse miktoarm stars is similar (see the Supporting Information for a quantitative comparison).

Guided by these SCFT simulations, we designed miktoarm star copolymers consisting of L and D arms targeting the volume fraction range where stable Frank–Kasper phases are predicted to form based on Figure 2. Procedurally, D macromonomers were prepared with a polymerizable norbornene end-group and L macroterminators with an ene–yne terminator moiety (Tables S1 and S2). The μSTAR synthesis was executed in two distinct steps within one pot (Figure 1, top). First, ring-opening metathesis polymerization of 3 or 4 equiv of D macromonomer relative to Grubbs' third generation catalyst yielded short stars with a controlled number of arms and an active Ru chain-end. Second, after full conversion of the D macromonomer, *in situ* termination with L macroterminator (1 equiv) formed LD$_3$ or LD$_4$ miktoarm stars. As discussed above, these values represent the average number of D arms around a distribution created from the statistical polymerization process in the first step.

https://doi.org/10.1021/acs.macromol.4c02202
Macromolecules XXXX, XXX, XXX–XXX

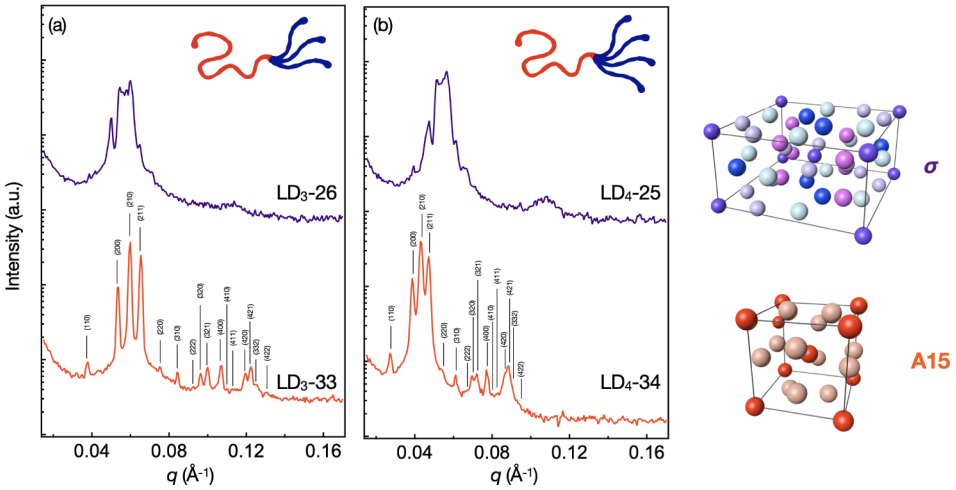

Figure 3. Experimental realization of Frank−Kasper σ and A15 phases in disperse mixtures of (a) LD_3 and (b) LD_4 miktoarm stars. Lines indicate allowed reflections for A15 ($Pm\bar{3}n$); indexing for σ ($P4_2/mnm$) is provided in the Supporting Information for clarity (Figure S9).

For each sample, the average number of D arms (n) was measured by ^{1}H NMR spectroscopy on an aliquot of the polymerized D macromonomer (D_n), which was extracted and quenched by ethyl vinyl ether following ROMP but before addition of the macroterminator (Table S3). Residual catalyst was removed using a metal scavenger prior to ^{1}H NMR measurements. Additional ^{1}H NMR and size-exclusion chromatography (SEC) analysis confirmed the stoichiometric coupling of D_n with L macroterminator. The volume fraction of the single L arm (f_L) was determined by integrating signals arising from L and D segments in the ^{1}H NMR spectra of the final miktoarm products. Detailed characterization is provided in (Figures S3−S7). Using D macromonomers and L macroterminators with different molecular weights, a library of disperse LD_3 and LD_4 miktoarm stars was prepared over a range of f_L (Table S4).

Synthesized miktoarm stars are denoted LD_n-*XX*, where n denotes the integer-rounded average number of arms and *XX* is the volume fraction $f_L \times 100\%$. For example, LD_3-33 corresponds to a sample with an experimentally determined average of 3 D arms and a volume fraction $f_L = 0.33$ for the L block. A library of disperse LD_3 samples (LD_3-26, LD_3-28, LD_3-30, LD_3-31, LD_3-33, LD_3-35, LD_3-39, and LD_3-42) and disperse LD_4 samples (LD_4-25, LD_4-30, LD_4-31, LD_4-34, LD_4-36, LD_4-39, and LD_4-43) highlights the good control over compositional and architectural variations enabled by μSTAR.

Based on our SCFT simulations, four representative samples (LD_3-26, LD_3-33, LD_4-25, and LD_4-34) were initially selected and subjected to an annealing process at 100 °C for 24 h, preceded by a quick equilibration at 180 °C for 5 min to induce disordering (detailed procedures and representative SAXS profiles at 180 °C are included in the Supporting Information). Following annealing and cooling to room temperature for a minimum of 24 h, small-angle X-ray scattering (SAXS) experiments were conducted. As shown in Figure 3, both disperse LD_3 and LD_4 miktoarm stars self-assemble into σ and A15 at volume fractions in quantitative agreement with SCFT. The resolution in all four SAXS profiles permitted indexing to the A15 and σ space groups (see also Figure S9). Additionally, for LD_3-33, we reconstructed the unit cell electron-density map via Le Bail refinement and charge flipping to clearly show a real-space depiction of the A15 structure (see Figure S10). These experimental results demonstrate that disperse LD_n miktoarm stars synthesized via the μSTAR platform can successfully self-assemble into Frank−Kasper phases, despite arm-number dispersity that arises from the ROMP mechanism. The formation of highly ordered A15 phases by LD_3 and LD_4 miktoarm stars is especially remarkable because previous LD_3 miktoarm stars with a precise number of each arm did not assemble into similarly clear Frank−Kasper structures.[19]

SCFT provides additional insight into the structure and distribution of disperse LD_n molecules in the A15 phase. There are two distinct sizes of micelles in the A15 structure, where the large and small ones possess 14 and 12 neighbors (defined as micelles whose Voronoi cells share a common facet), respectively. We find that LD_n molecules with smaller n disproportionally contribute to the formation of the large micelles. For example, at $f_L = 0.289$, within the interior of a small micelle (we consider spatial locations with $\rho_L > 0.5$ to be the interior of micelles when performing segmentation of the structure) the L block in LD, LD_2, LD_3, LD_4, and LD_5 molecules constitutes 4.66%, 24.76%, 42.51%, 23.74%, and 4.34% of the L-species density, respectively, whereas within the interior of each large micelle the L block represents 5.01%, 25.17%, 42.08%, 23.41%, and 4.32% of the L-species density, respectively. We note that with precise analogues, the volume asymmetry of distinct micelles must come from a different *number* of molecules in each. In contrast, with disperse systems, such volume asymmetry can arise from the aforementioned molecular partitioning, reducing the need for chain exchange between different micelles and potentially leading to accelerated self-assembly kinetics and improved ordering. Collectively, these findings prompted us to further investigate whether A15 similarly forms across a wide range of volume fractions f_L as predicted by SCFT.

Phase Portraits of Disperse LD_3 and LD_4 Miktoarm Stars. Using the library of LD_3 and LD_4 samples, we next determined the range of f_L over which A15 is experimentally stable. Figure 4 shows SAXS patterns for samples with f_L = 0.26−0.42 (detailed reflection indexing is presented in Figure S12). These results indicate a significant window of A15 stability extending from $f_L = 0.30$ to 0.39. Most of these samples have clear and sharp reflections with the exception of LD_3-39 that is broader but nevertheless consistent with A15 indexing. Near the lower boundary of the A15 window, LD_3-28

https://doi.org/10.1021/acs.macromol.4c02202
Macromolecules XXXX, XXX, XXX−XXX

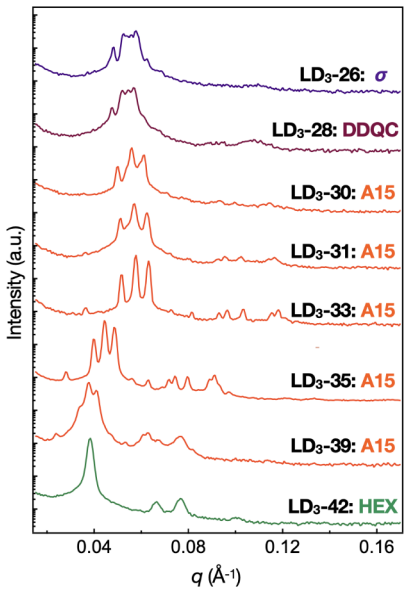

Figure 4. SAXS profiles of disperse LD_3 miktoarm star polymers across a range of different f_L (see Figure S12 for indexing); the stability of σ and A15 is evident.

was observed to form a dodecagonal quasicrystal (DDQC).[26−28] Interestingly, the σ phase can be viewed as a periodic approximant to an aperiodic DDQC structure.[26] A long-lived metastable DDQC mesophase near the σ−A15 phase boundary has also been experimentally observed in a previous study of miktoarm stars.[23]

Similar results were obtained with disperse LD_4 samples, namely, a sequence of σ−DDQC−A15−HEX phases as f_L increases (Figure S13). SAXS analysis again revealed a well-ordered A15 phase in LD_4-31, LD_4-34, and LD_4-36 as evidenced by characteristic scattering peaks. However, LD_4-39 exhibited even broader reflections than LD_3-39 (Figure S13f), which is indicative of a kinetically trapped liquid-like micellar packing (LLP) state often encountered in the formation of Frank−Kasper phases.[19,26,29−31] The observation of LLP suggests LD_4-39 may ultimately resolve into a well-defined A15 morphology. One factor that may contribute to this more pronounced kinetic limitation compared to the corresponding LD_3 sample is an increase in n and molecular weight. Nevertheless, LD_4 clearly self-assembles into Frank−Kasper phases that are analogous to LD_3.

Experimentally, the phase behavior of LD_n systems is summarized in Figure 5. Note that data for a precise LD diblock copolymer was derived from literature.[4] This portrait reveals a significant shift in both the σ−A15 and A15−HEX phase boundaries as n increases, with a particularly pronounced change observed between LD and LD_3. Next, we probe the origin of this behavior using SCFT simulations.

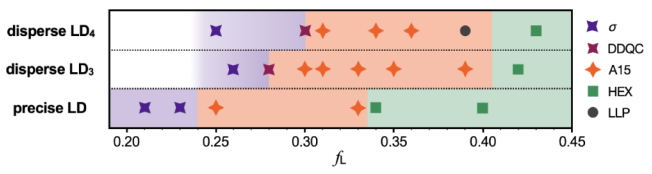

Figure 5. Differences in order−order transitions as a function of arm number n: precise LD, disperse LD_3, and disperse LD_4. Note that the LD diblock data is from previous work.[4]

SCFT Insights into the Effects of Conformational Asymmetry. Experimentally, as the number of D arms n increases, some order−order phase boundaries shift markedly to higher f_L for disperse LD_n miktoarm stars. This is similar to observations for AB_n miktoarm stars with precise n that were reported in recent experimental work.[19,23] It is also consistent with strong stretching theory,[21] where a single parameter $\epsilon = n \cdot (b_A/b_B)$ was thought to capture the degree of conformational asymmetry. However, notably, exceptions with respect to strong stretching theory do exist, e.g., the σ−A15 phase boundary deflects to lower f_A for AB linear diblock copolymers as b_A/b_B increases.[4]

To fully understand the effects of different types of conformational asymmetry on the phase behavior of AB_n miktoarm star polymers, we performed two sets of SCFT simulations. Specifically, we (i) varied n while fixing b_A/b_B, and (ii) varied b_A/b_B while fixing n, both at constant segregation strength χN_{tot}, where N_{tot} is the total degree of polymerization for a miktoarm star. Since the phase behavior of precise and disperse AB_n systems is similar as mentioned above, for simplicity, these simulations were performed with precise AB_n. As shown in Figure 6a, as n increases at fixed b_A/b_B, the σ−A15

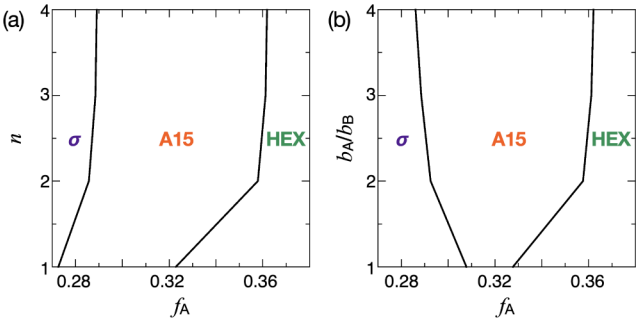

Figure 6. SCFT simulations predict opposite trends in the σ−A15 boundary for the two contributions to conformational asymmetry and similar trends in the A15−HEX boundary. (a) n effects at $b_A/b_B = 3$ and $\chi N_{tot} = 38$. (b) b_A/b_B effects at $n = 3$, $\chi N_{tot} = 38$.

phase boundary deflects to higher f_A, while the opposite is true as b_A/b_B increases at fixed n, Figure 6b. The former case, Figure 6a, is consistent with our experimental observations (recall Figure 5). These results clearly demonstrate the opposing influence of the two types of conformational asymmetry on the equilibrium phase behavior of AB_n miktoarm stars, which strong segregation theory fails to describe. We believe this is because the theory[21] assumes a circular or spherical unit cell around each micelle for the HEX and sphere phases and does not take into account how micelles pack; thus, it cannot be used to predict whether one sphere phase is more stable than another sphere phase, e.g., the relative stability of BCC, σ, and A15. On the other hand, the A15−HEX phase boundary is deflected to higher f_A as n or b_A/b_B increases, which is consistent with the prediction of strong-stretching theory[21] and different from the case of the σ−A15 phase boundary.

Accelerating Self-Assembly Kinetics with Nonselective Solvent. Although we identified a remarkably wide window of A15 stability in both disperse LD_3 and LD_4, as previously mentioned, two samples with the highest f_L near the A15−HEX boundary (LD_3-39 and LD_4-39) exhibited broad SAXS reflections indicative of poor ordering, likely due to kinetic trapping. Because of the similarity in behavior between

https://doi.org/10.1021/acs.macromol.4c02202
Macromolecules XXXX, XXX, XXX−XXX

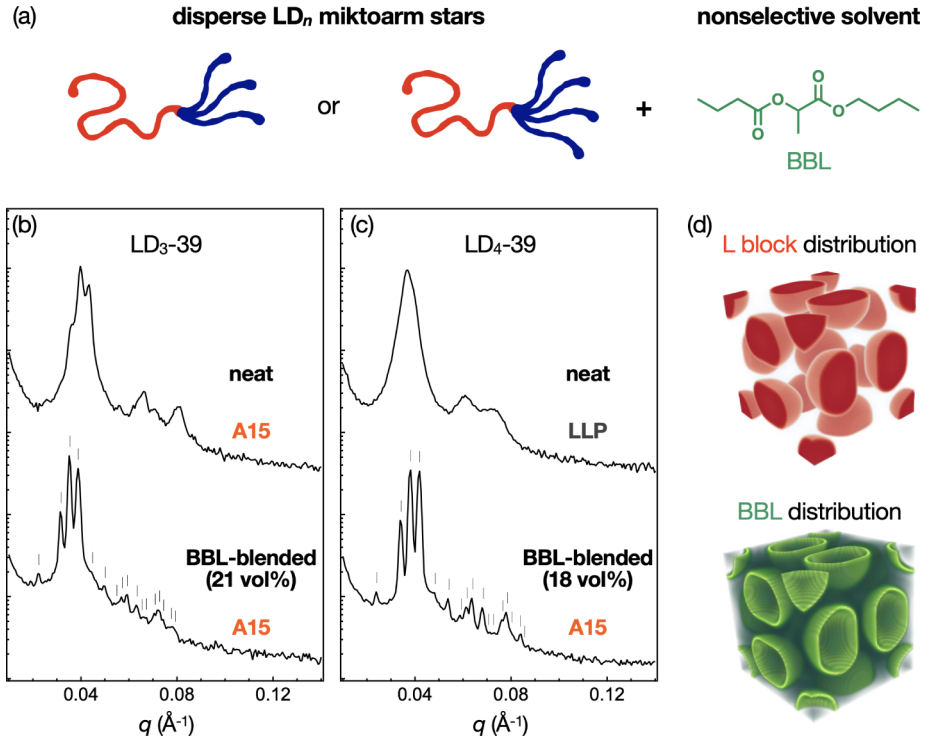

Figure 7. (a) Schematic representation of blending nonselective solvent BBL with disperse LD_n miktoarm stars to improve ordering. (b,c) SAXS patterns of (b) LD_3-39 and (c) LD_4-39 obtained at 100 °C indicate BBL blending significantly improves the ordering of A15. (d) SCFT simulations demonstrate the distribution of BBL (21 vol %) is almost uniform with a slight accumulation at the interface of L-rich micelles and D-rich matrix in the A15 phase formed by an LD_3 miktoarm star at f_L = 0.39.

these two distinct but related materials, we were motivated to try different annealing conditions to improve the ordering. More generally, kinetic limitations often pose significant challenges in achieving highly ordered Frank−Kasper phases,[19,26,29−31] particularly when dealing with copolymers having complex architectures,[19,32−34] so these efforts might reveal processing strategies that extend to other systems as well.

To address this challenge, we explored a solvent addition process aimed at facilitating the formation of high-quality Frank−Kasper phases with LD_3-39 and LD_4-39. The approach involved introducing a nonselective good solvent for both the L and D blocks, which is intended to lower the glass-transition temperature of the polymers and improve chain mobility[35] without inducing selective segregation that would shift volume fractions.[36,37] An ideal choice of solvent would have a high boiling point and low vapor pressure to avoid complexities related to solvent evaporation.[38] Upon screening various small molecules, we selected butyl butyryllactate (BBL), which has a boiling point of 250 °C at standard pressure and a vapor pressure of 2 Pa at 25 °C. Using Small's method,[39] the solubility parameters δ (in units of $cal^{1/2}$ $cm^{-3/2}$) of BBL, L, and D were calculated to be 8.77, 9.57 and 8.40, respectively; see the Supporting Information for details. The solubility parameter of BBL therefore lies in between that of the L and D blocks, with a value sufficiently close to both such that it is expected to be approximately nonselective.

Procedurally, a solution of BBL in DCM was added to LD_3-39 or LD_4-39 followed by complete evaporation of the DCM as confirmed by ^{1}H NMR. Each sample was then subjected to annealing at 100 °C for 24 h; see the Supporting Information for details. Figure 7 compares the SAXS patterns of LD_3-39 and LD_4-39 at 100 °C before and after blending. A significant improvement in the number of peaks and their sharpness was observed in both cases by blending approximately 20 vol % of BBL.

To further elucidate the role of BBL in facilitating the self-assembly of miktoarm stars, we conducted an SCFT simulation of the A15 phase formed by LD_3 in a solution of 21% BBL—the same composition used experimentally for LD_3-39 (see the Supporting Information for details). The solvent (denoted as S) was assumed to be athermal, i.e., $\chi_{LS} = \chi_{DS} = 0$, since the solubility parameter of BBL is close to those of L and D segments as mentioned above. As shown by a visualization of the SCFT-relaxed structures in Figure 7d, the local volume fraction of BBL varies from 20% to 23% at different spatial locations, i.e., the distribution of BBL is almost uniform with a slight accumulation at the interface of L-rich micelles and D-rich matrix. The dominant effect of a nonselective athermal solvent is therefore to screen unfavorable L−D interactions, leading to a reduced effective Flory−Huggins interaction parameter. In addition, we note that within the unit cell of an A15 structure, there are 6 large micelles and 2 small micelles, which appear to be nonspherical. We quantified shape sphericity of the micelles using the isoperimetric quotient[4] $IQ \equiv 36\pi V^2/A^3$, where V and A are the volume and surface area of a micelle, respectively, with spatial locations having $\rho_L > 0.5$ considered to be the interior of micelles when performing segmentation of the structure. Note that IQ = 1 corresponds to a sphere. The isoperimetric quotient IQ for the large and small micelles was determined to be 0.940 and 0.989 after the addition of BBL, and 0.936 and 0.983 without BBL, respectively. In other words, the micelles become slightly more spherical after the addition of BBL, leading to reduced

https://doi.org/10.1021/acs.macromol.4c02202
Macromolecules XXXX, XXX, XXX−XXX

surface tension since a sphere is well-known to possess the least surface area for a given volume among all shapes. These results are consistent with observations from previous experimental and computational studies of traditional block copolymer morphologies containing nonselective good solvent.[36,40−43] This method holds promise for overcoming kinetic issues commonly encountered with Frank−Kasper phases formed from polymers having complex architectures and block sequences.

CONCLUSIONS

In this work, we leveraged a synergistic combination of SCFT simulations and experimental techniques to discover Frank−Kasper phases in AB_n miktoarm star polymers having inherent dispersity in n. Specifically, for LD_3 and LD_4 miktoarm stars with L = poly(*rac*-lactide) and D = poly(dodecyl acrylate), dispersity in the number of D arms still yields a wide range of volumes fractions f_L over which well-ordered σ and A15 phases form. As n increases, order−order phase boundaries were found to deflect toward larger f_L, which is consistent with the number of arms dominating conformational asymmetry effects rather than the ratio of statistical segment lengths b_L/b_D. This result challenges the conventional thinking that a single parameter $\epsilon = n \cdot (b_A/b_B)$ can fully describe the effects of conformational asymmetry in AB_n miktoarm star systems. Finally, reproducibly sluggish self-assembly kinetics observed with samples near the A15−HEX boundary were significantly accelerated by the addition of nonselective solvent, demonstrating a processing route that may prove broadly useful in the context of Frank−Kasper phases. In summary, μSTAR is a powerful technique that can be used to synthesize disperse mixtures of miktoarm stars with self-assembly that closely resembles precise analogues.

ASSOCIATED CONTENT

Supporting Information

The Supporting Information is available free of charge at https://pubs.acs.org/doi/10.1021/acs.macromol.4c02202.

SCFT simulation details; materials preparation; synthesis; SAXS studies; calculation of solubility parameters (PDF)

AUTHOR INFORMATION

Corresponding Authors

Duyu Chen − *Materials Research Laboratory, University of California, Santa Barbara, California 93106, United States*; Email: duyu@ucsb.edu

Glenn H. Fredrickson − *Materials Research Laboratory and Department of Chemical Engineering, University of California, Santa Barbara, California 93106, United States*; orcid.org/0000-0002-6716-9017; Email: ghf@mrl.ucsb.edu

Christopher M. Bates − *Materials Research Laboratory and Materials Department, University of California, Santa Barbara, California 93106, United States*; orcid.org/0000-0002-1598-794X; Email: cbates@ucsb.edu

Authors

Kodai Watanabe − *Materials Research Laboratory, University of California, Santa Barbara, California 93106, United States*

Yongsi Zhu − *Department of Chemistry & Biochemistry, University of California, Santa Barbara, California 93106, United States*

Devon Callan − *Department of Chemical Engineering, University of California, Santa Barbara, California 93106, United States*

Complete contact information is available at: https://pubs.acs.org/10.1021/acs.macromol.4c02202

Author Contributions

#K.W. and D.C. contributed equally to this work.

Notes

The authors declare no competing financial interest.

ACKNOWLEDGMENTS

This work was primarily supported by the U.S. Department of Energy, Office of Basic Energy Sciences, under Award Number DE-SC0019001. This work made use of the BioPACIFIC Materials Innovation Platform computing resources of the National Science Foundation Award No. DMR-1933487. Use was also made of computational facilities purchased with funds from the National Science Foundation (OAC-1925717 and CNS-1725797) and administered by the Center for Scientific Computing (CSC). The CSC is supported by the California NanoSystems Institute and the Materials Research Science and Engineering Center (MRSEC; NSF DMR-2308708) at UC Santa Barbara.

REFERENCES

(1) Frank, F. C.; Kasper, J. S. Complex Alloy Structures Regarded as Sphere Packings. I. Definitions and Basic Principles. *Acta Crystallogr.* **1958**, *11*, 184−190.

(2) Frank, F. C.; Kasper, J. S. Complex Alloy Structures Regarded as Sphere Packings. II. Analysis and Classification of Pepresentative Structures. *Acta Crystallogr.* **1959**, *12*, 483−499.

(3) Lee, S.; Bluemle, M. J.; Bates, F. S. Discovery of a Frank−Kasper σ Phase in Sphere-Forming Block Copolymer Melts. *Science* **2010**, *330*, 349−353.

(4) Bates, M. W.; Lequieu, J.; Barbon, S. M.; Lewis, R. M.; Delaney, K. T.; Anastasaki, A.; Hawker, C. J.; Fredrickson, G. H.; Bates, C. M. Stability of the A15 Phase in Diblock Copolymer Melts. *Proc. Natl. Acad. Sci. U.S.A.* **2019**, *116*, 13194−13199.

(5) Grason, G. M.; DiDonna, B. A.; Kamien, R. D. Geometric Theory of Diblock Copolymer Phases. *Phys. Rev. Lett.* **2003**, *91*, 058304.

(6) Grason, G. M.; Kamien, R. D. Interfaces in Diblocks: A Study of Miktoarm Star Copolymers. *Macromolecules* **2004**, *37*, 7371−7380.

(7) Xie, N.; Li, W.; Qiu, F.; Shi, A.-C. σ Phase Formed in Conformationally Asymmetric AB-Type Block Copolymers. *ACS Macro Lett.* **2014**, *3*, 906−910.

(8) Lequieu, J.; Koeper, T.; Delaney, K. T.; Fredrickson, G. H. Extreme Deflection of Phase Boundaries and Chain Bridging in $A(BA')_n$ Miktoarm Star Polymers. *Macromolecules* **2020**, *53*, 513−522.

(9) Lee, S.; Leighton, C.; Bates, F. S. Sphericity and Symmetry Breaking in the Formation of Frank−Kasper Phases from One Component Materials. *Proc. Natl. Acad. Sci. U. S. A.* **2014**, *111*, 17723−17731.

(10) Yan, X.-Y.; Liu, Y.; Liu, X.-Y.; Lei, H.; Li, X.-H.; Wang, Y.; Li, W.; Guo, Q.-Y.; Huang, M.; Cheng, S. Z. D. Guidelines for Superlattice Engineering with Giant Molecules: The Pivotal Role of Mesoatoms. *Phys. Rev. Mater.* **2023**, *7*, 120302.

(11) Su, Z.; Hsu, C.-H.; Gong, Z.; Feng, X.; Huang, J.; Zhang, R.; Wang, Y.; Mao, J.; Wesdemiotis, C.; Li, T. Identification of a Frank−Kasper Z phase from shape amphiphile self-assembly. *Nat. Chem.* **2019**, *11* (10), 899−905.

(12) Tsai, C. L.; Fredrickson, G. H. Using particle swarm optimization and self-consistent field theory to discover globally stable morphologies of block copolymers. *Macromolecules* **2022**, *55*, 5249−5262.
(13) Zhao, M.; Li, W. Laves phases formed in the binary blend of AB_4 miktoarm star copolymer and A-homopolymer. *Macromolecules* **2019**, *52*, 1832−1842.
(14) Dorfman, K. D. Frank-Kasper Phases in Block Polymers. *Macromolecules* **2021**, *54*, 10251−10270.
(15) Lewis, R. M., III; Arora, A.; Beech, H. K.; Lee, B.; Lindsay, A. P.; Lodge, T. P.; Dorfman, K. D.; Bates, F. S. Role of Chain Length in the Formation of Frank−Kasper Phases in Diblock Copolymers. *Phys. Rev. Lett.* **2018**, *121*, 208002.
(16) Barbon, S. M.; Song, J.-A.; Chen, D.; Zhang, C.; Lequieu, J.; Delaney, K. T.; Anastasaki, A.; Rolland, M.; Fredrickson, G. H.; Bates, M. W.; Hawker, C. J.; Bates, C. M. Architecture Effects in Complex Spherical Assemblies of $(AB)_n$-Type Block Copolymers. *ACS Macro Lett.* **2020**, *9*, 1745−1752.
(17) Vigil, D. L.; Quah, T.; Sun, D.; Delaney, K. T.; Fredrickson, G. H. Self-Consistent Field Theory Predicts Universal Phase Behavior for Linear, Comb, and Bottlebrush Diblock Copolymers. *Macromolecules* **2022**, *55*, 4237−4244.
(18) Le, A. N.; Liang, R.; Ji, X.; Fu, X.; Zhong, M. Random Copolymerization of Macromonomers as a Versatile Strategy to Synthesize Mixed-Graft Block Copolymers. *J. Polym. Sci.* **2021**, *59*, 2571−2580.
(19) Bates, M. W.; Barbon, S. M.; Levi, A. E.; Lewis Iii, R. M.; Beech, H. K.; Vonk, K. M.; Zhang, C.; Fredrickson, G. H.; Hawker, C. J.; Bates, C. M. Synthesis and Self-Assembly of AB_n Miktoarm Star Polymers. *ACS Macro Lett.* **2020**, *9*, 396−403.
(20) Chen, D.; Quah, T.; Delaney, K. T.; Fredrickson, G. H. Investigation of the Self-Assembly Behavior of Statistical Bottlebrush Copolymers via Self-Consistent Field Theory Simulations. *Macromolecules* **2022**, *55*, 9324−9333.
(21) Milner, S. T. Chain Architecture and Asymmetry in Copolymer Microphases. *Macromolecules* **1994**, *27*, 2333−2335.
(22) Liu, M.; Blankenship, J. R.; Levi, A. E.; Fu, Q.; Hudson, Z. M.; Bates, C. M. Miktoarm Star Polymers: Synthesis and Applications. *Chem. Mater.* **2022**, *34*, 6188−6209.
(23) Sun, Y.; Tan, R.; Ma, Z.; Gan, Z.; Li, G.; Zhou, D.; Shao, Y.; Zhang, W.-B.; Zhang, R.; Dong, X.-H. Discrete Block Copolymers with Diverse Architectures: Resolving Complex Spherical Phases with One Monomer Resolution. *ACS Cent. Sci.* **2020**, *6*, 1386−1393.
(24) Levi, A. E.; Fu, L.; Lequieu, J.; Horne, J. D.; Blankenship, J.; Mukherjee, S.; Zhang, T.; Fredrickson, G. H.; Gutekunst, W. R.; Bates, C. M. Efficient Synthesis of Asymmetric Miktoarm Star Polymers. *Macromolecules* **2020**, *53*, 702−710.
(25) Blankenship, J. R.; Levi, A. E.; Goldfeld, D. J.; Self, J. L.; Alizadeh, N.; Chen, D.; Fredrickson, G. H.; Bates, C. M. Asymmetric Miktoarm Star Polymers as Polyester Thermoplastic Elastomers. *Macromolecules* **2022**, *55*, 4929−4936.
(26) Gillard, T. M.; Lee, S.; Bates, F. S. Dodecagonal Quasicrystalline Order in a Diblock Copolymer Melt. *Proc. Natl. Acad. Sci. U.S.A.* **2016**, *113*, 5167−5172.
(27) Schulze, M. W.; Lewis, R. M.; Lettow, J. H.; Hickey, R. J.; Gillard, T. M.; Hillmyer, M. A.; Bates, F. S. Conformational Asymmetry and Quasicrystal Approximants in Linear Diblock Copolymers. *Phys. Rev. Lett.* **2017**, *118*, 207801.
(28) Feng, X.; Liu, G.; Guo, D.; Lang, K.; Zhang, R.; Huang, J.; Su, Z.; Li, Y.; Huang, M.; Li, T.; Cheng, S. Z. D. Transition Kinetics of Self-Assembled Supramolecular Dodecagonal Quasicrystal and Frank−Kasper σ Phases in AB_n Dendron-Like Giant Molecules. *ACS Macro Lett.* **2019**, *8*, 875−881.
(29) Kim, K.; Schulze, M. W.; Arora, A.; Lewis Iii, R. M.; Hillmyer, M. A.; Dorfman, K. D.; Bates, F. S. Thermal processing of diblock copolymer melts mimics metallurgy. *Science* **2017**, *356*, 520−523.
(30) Kim, K.; Arora, A.; Lewis Iii, R. M.; Liu, M.; Li, W.; Shi, A.-C.; Dorfman, K. D.; Bates, F. S. Origins of low-symmetry phases in asymmetric diblock copolymer melts. *Proc. Natl. Acad. Sci. U.S.A.* **2018**, *115*, 847−854.
(31) Dorfman, K. D.; Wang, Z.-G. Liquid-Like States in Micelle-Forming Diblock Copolymer Melts. *ACS Macro Lett.* **2023**, *12*, 980−985.
(32) Chang, A. B.; Bates, F. S. Impact of Architectural Asymmetry on Frank-Kasper Phase Formation in Block Polymer Melts. *ACS Nano* **2020**, *14*, 11463−11472.
(33) Feng, X.; Liu, G.; Guo, D.; Lang, K.; Zhang, R.; Huang, J.; Su, Z.; Li, Y.; Huang, M.; Li, T.; Cheng, S. Z. D. Transition Kinetics of Self-Assembled Supramolecular Dodecagonal Quasicrystal and Frank-Kasper σ Phases in ABn Dendron-Like Giant Molecules. *ACS Macro Lett.* **2019**, *8*, 875−881.
(34) Chiu, W.-C.; Cheng, Y.-H.; Lin, J.-H.; Tung, C.-H.; Nishimura, T.; Chen, C.-Y.; Isono, T.; Satoh, T.; Chen, H.-L. Tuning the Complex Spherical Phase of Sugar-Based Block Co-Oligomer via Single-Monomer-Mediated Composition Variation. *Macromolecules* **2024**, *57* (13), 6076−6089.
(35) Gutierrez, M. H.; Ford, W. T. The glass-to-gel transition in solvent-swollen polystyrene networks. *J. Polym. Sci., Part A: polym. Chem.* **1986**, *24*, 655−663.
(36) Lo, T.-Y.; Chao, C.-C.; Ho, R.-M.; Georgopanos, P.; Avgeropoulos, A.; Thomas, E. L. Phase transitions of polystyrene-b-poly (dimethylsiloxane) in solvents of varying selectivity. *Macromolecules* **2013**, *46*, 7513−7524.
(37) Chang, C.-Y.; Manesi, G.-M.; Yang, C.-Y.; Hung, Y.-C.; Yang, K.-C.; Chiu, P.-T.; Avgeropoulos, A.; Ho, R.-M. Mesoscale networks and corresponding transitions from self-assembly of block copolymers. *Proc. Natl. Acad. Sci. U. S. A.* **2021**, *118*, e2022275118.
(38) Kim, S. H.; Misner, M. J.; Xu, T.; Kimura, M.; Russell, T. P. Highly oriented and ordered arrays from block copolymers via solvent evaporation. *Adv. Mater.* **2004**, *16*, 226−231.
(39) Small, P. A. Some factors affecting the solubility of polymers. *J. Appl. Chem.* **1953**, *3*, 71−80.
(40) Lodge, T. P.; Hamersky, M. W.; Hanley, K. J.; Huang, C.-I. Solvent distribution in weakly-ordered block copolymer solutions. *Macromolecules* **1997**, *30*, 6139−6149.
(41) Fredrickson, G. H.; Leibler, L. Theory of block copolymer solutions: nonselective good solvents. *Macromolecules* **1989**, *22*, 1238−1250.
(42) Hanley, K. J.; Lodge, T. P.; Huang, C.-I. Phase behavior of a block copolymer in solvents of varying selectivity. *Macromolecules* **2000**, *33*, 5918−5931.
(43) Whitmore, M. D.; Vavasour, J. D. Self-consistent mean field theory of the microphase diagram of block copolymer/neutral solvent blends. *Macromolecules* **1992**, *25*, 2041−2045.

https://doi.org/10.1021/acs.macromol.4c02202
Macromolecules XXXX, XXX, XXX−XXX